



University of HUDDERSFIELD

University of Huddersfield Repository

Ipatova, I., Harrison, Robert W., Terentyev, D., Donnelly, Stephen E. and Jimenez-Melero, E.

Thermal Evolution of the Proton Irradiated Structure in Tungsten–5 wt% Tantalum

Original Citation

Ipatova, I., Harrison, Robert W., Terentyev, D., Donnelly, Stephen E. and Jimenez-Melero, E. (2017) Thermal Evolution of the Proton Irradiated Structure in Tungsten–5 wt% Tantalum. *Journal of Fusion Energy*, 36 (6). pp. 234-239. ISSN 0164-0313

This version is available at <http://eprints.hud.ac.uk/id/eprint/34081/>


The University Repository is a digital collection of the research output of the University, available on Open Access. Copyright and Moral Rights for the items on this site are retained by the individual author and/or other copyright owners. Users may access full items free of charge; copies of full text items generally can be reproduced, displayed or performed and given to third parties in any format or medium for personal research or study, educational or not-for-profit purposes without prior permission or charge, provided:

- The authors, title and full bibliographic details is credited in any copy;
- A hyperlink and/or URL is included for the original metadata page; and
- The content is not changed in any way.

For more information, including our policy and submission procedure, please contact the Repository Team at: E.mailbox@hud.ac.uk.

<http://eprints.hud.ac.uk/>

Thermal Evolution of the Proton Irradiated Structure in Tungsten–5 wt% Tantalum

I. Ipatova^{1,2}  · R. W. Harrison³ · D. Terentyev⁴ · S. E. Donnelly³ · E. Jimenez-Melero¹

Published online: 11 November 2017

© The Author(s) 2017. This article is an open access publication

Abstract We have monitored the thermal evolution of the proton irradiated structure of W–5 wt% Ta alloy by in-situ annealing in a transmission electron microscope at fusion reactor temperatures of 500–1300 °C. The interstitial-type $a/2\langle 111 \rangle$ dislocation loops emit self-interstitial atoms and glide to the free sample surface during the early stages of annealing. The resultant vacancy excess in the matrix originates vacancy-type $a/2\langle 111 \rangle$ dislocation loops that grow by loop and vacancy absorption in the temperature range of 600–900 °C. Voids form at 1000 °C, by either vacancy absorption or loop collapse, and grow progressively up to 1300 °C. Tantalum delays void formation by a vacancy-solute trapping mechanism.

Keywords Refractory metals · Radiation damage · Lattice defects · Annealing · Transmission electron microscopy

Introduction

Tungsten and its alloys are the prime structural and armour material candidates for high-heat load components facing the hydrogen plasma in nuclear fusion reactors [1–3], due

to their unique thermal conductivity and high-temperature strength, in combination with low surface sputtering yields and resistance to radiation-induced swelling [4–6]. The thermal loads on plasma-facing components are predicted to be 0.1–20 MW/m² during steady-state reactor operation [7, 8], and even values close to GW/m² range during off-normal events such as plasma disruptions and edge localised events [9]. The expected lowest shield temperatures for W-based armour materials range from ~ 500 °C in the blanket's first wall to > 800–900 °C in helium-cooled divertor designs and even > 1700 °C in the divertor armour surface [1].

Unfortunately, tungsten manifests an intrinsic brittleness at low temperatures, with reported values of the ductile-to-brittle transition temperature (DBTT) in the range of 250–350 °C, depending on its microstructure and processing route [10, 11]. Neutron irradiation is reported to increase the DBTT up to ~ 800–1000 °C [12, 13]. In plasma-facing components of fusion reactors, the high neutron fluxes are predicted to induce radiation damage rates of 3–30 dpa/year [8]. Besides that, neutron bombardment will also cause the transmutation of W into Re and subsequently Os, and therefore trigger the formation of brittle σ (ReW) and χ (WRe₃) precipitates [14, 15]. The radiation-induced embrittlement stemming from lattice defects and brittle phases will continuously reduce the recommended temperature window for safe operation of W-based components [13], and potentially cause premature failure during low-temperature reactor operations [16].

In this work, we have assessed the radiation-induced lattice damage in W–5 wt% Ta (W–5Ta) alloy at the relatively low temperature of 350 °C, and how the damaged structure evolves during annealing up to 1300 °C. Tantalum additions to tungsten, either in solid solution or as short fibres, can potentially increase its ductility [1, 17] and

✉ I. Ipatova
iuliia.ipatova@postgrad.manchester.ac.uk

¹ School of Materials, The University of Manchester, Oxford Road, Manchester M13 9PL, UK

² Dalton Cumbrian Facility, The University of Manchester, Moor Row CA24 3HA, UK

³ School of Computing and Engineering, University of Huddersfield, Huddersfield HD1 3DH, UK

⁴ Nuclear Materials Science Institute, SCK-CEN, Boeretang 200, 2400 Mol, Belgium

also delay the formation of brittle phases stemming from the neutron-induced transmutation sequence [14]. Recent reports on self-ion irradiations of W–Ta alloys at temperatures ≤ 500 °C and up to a damage level of 33 dpa confirm the absence of radiation-induced Ta clustering. Moreover, the presence of Ta hinders the formation of Re clusters under irradiation [18]. Interstitial-type dislocation loops form at those low irradiation temperatures in W–Ta alloys. The loop size is smaller and the loop number density is higher than in tungsten under equivalent irradiation conditions [19]. The low-temperature irradiation-hardening due to dislocation loops saturates at a damage level of 13 dpa at 300 °C [20]. Ta is predicted to have a repulsive interaction with self-interstitial atom (SIA) defects such as $\langle 111 \rangle$ crowdion [21] and dumbbell [22] configurations, and potentially restrict the mobility of SIAs and interstitial loops in W [19].

Experimental Details

The as-received W–5Ta material was initially annealed in vacuum ($\sim 10^{-5}$ mbar) at 1400 °C for 2 h for recrystallization. A 3 mm-diameter TEM disc was prepared by mechanical pre-thinning, followed by electropolishing at a temperature of ~ -5 °C, using a Struers Tenupol-5 unit and an electrolyte comprising 15 vol% sulphuric acid (95%) and 85 vol% methanol. The TEM disc was proton irradiated at the Microscope and Ion Accelerator for Materials Investigations (MIAMI-1 facility) located at the University of Huddersfield [23]. The sample was placed in a high-temperature Gatan 652 double-tilt specimen holder, and then mounted in a JEOL JEM-2000FX TEM operating at an accelerating voltage of 200 kV. This microscope is installed at the end of a beam line connected to an electrostatic ion accelerator. The 40 keV proton irradiation was performed at a temperature of 350(2) °C, up to a damage level of 0.7 dpa and a fluence of 9.7×10^{17} ions/cm². The proton irradiated structure was characterised at room temperature using an FEI Tecnai T20 Transmission Electron microscope with LaB₆ crystal, equipped with a double-tilt specimen holder and operating at 200 kV. The determination of the Burgers vector \mathbf{b} of the observed dislocations made use of the $\mathbf{g} \cdot \mathbf{b} = 0$ invisibility criterion, where \mathbf{g} denotes the scattering vector. The nature of the dislocation loops was determined using the inside–outside contrast method. The foil thickness was derived from the fringes spacing of the convergent beam electron diffraction pattern, and was used to obtain the dislocation density applying graphical method [24].

Afterwards, the evolution of the proton irradiated structure was monitored in-situ during annealing using the same 200 kV JEOL JEM-2000FX TEM and the heating

Gatan 652 double-tilt specimen holder. The disc was first heated from room temperature up to 500 °C at a rate of 100 °C/min, and thereafter in steps of 100 °C up to 1300 °C at a lower rate of 50 °C/min. After each temperature step, the disc was maintained at a constant temperature for a period of 20 min, and TEM images were taken close to the [111] zone axis of the bcc structure of W–5Ta. Void analysis of the bright-field images was based on the “out-of-focus” imaging technique, where voids appear as white dots surrounded by black Fresnel fringes when recorded in an under-focused condition, and as dark dots with bright fringes in an over-focused condition [24]. Once the maximum temperature of 1300 °C was reached, the disc was cooled to room temperature, and the annealed structure analysed using the FEI Tecnai T20 Transmission electron microscope.

Results and Discussion

Dislocation Structure

The structure of the proton irradiated W–5Ta alloy is shown in Fig. 1, together with its evolution during post irradiation annealing up to 1300 °C. The as-irradiated microstructure is characterized by the presence of interstitial dislocation loops with a Burgers vector $a/2\langle 111 \rangle$. The average loop diameter is 33(2) nm and the number density takes a value of 2.2×10^{21} m⁻³. In contrast, the microstructure annealed at 1300 °C presents a lower dislocation density of 0.3×10^{21} m⁻³ and the average loop diameter is 26(1) nm. The Burgers vector of the loops after annealing is still $a/2\langle 111 \rangle$, however, the ellipsoidal shaped loops were determined to be of vacancy-type. The irradiated structure in bcc metals is characterized by a relatively large fraction of individual vacancy and self-interstitial atom (SIA) defects, together with a number of small mobile SIAs clusters, according to molecular dynamic simulations [25]. The enthalpy of migration of SIAs in tungsten equals to 85 meV [26, 27], and SIAs are mobile at temperatures as low as -253 °C corresponding to annealing stage I [28, 29]. Both the free surface of the sample and the interstitial dislocation loops act as biased sinks for mobile SIAs [30]. Furthermore, an attractive image force is generated that drives the dislocation loops towards the surface [31]. Small interstitial $a/2\langle 111 \rangle$ loops have recently been observed to hop in one-dimension during in-situ isochronal annealing of a TEM tungsten disc, previously irradiated with a 2 MeV W⁺ beam to a ion fluence of 10^{14} W⁺/cm². The loop hopping is significant at temperatures in the range of 300–700 °C, with increasing hopping frequency with temperature, and leads to loop loss to the sample surface [32]. Besides that, detrapping of SIAs

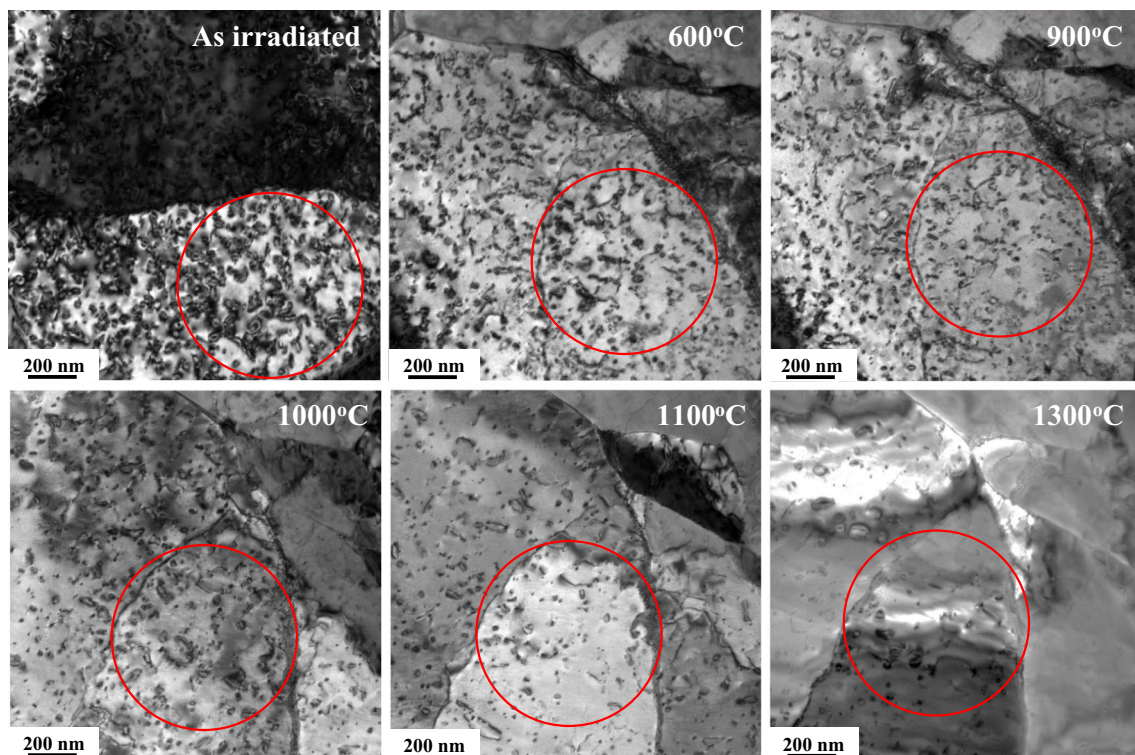


Fig. 1 Dislocation loop evolution in W-5Ta alloy during annealing, after proton irradiation at a temperature of 350 °C and a damage level of 0.7 dpa

from dislocations occurs in tungsten in the annealing stage II at -170 to 430 °C [28]. Therefore, the interstitial-type $a/2\langle 111 \rangle$ loops observed in the ‘as-irradiated’ structure of W-5Ta are not stable below 500 °C, and either glide towards the sample surface and/or lose SIAs, who may also migrate and become trapped at the free surface.

The migration of SIAs and interstitial dislocation loops towards the surface generates an excess of vacancies in near-surface regions of the sample [33]. Vacancy migration takes place in tungsten during the annealing stage III, corresponding to the temperature range of 430 – 650 °C [28, 34]. This range is shifted towards lower temperatures with increasing neutron fluence [35]. The activation enthalpy of long-range vacancy migration in tungsten is reported to be 1.7 – 2.0 eV [36, 37]. In fact, significant migration of single vacancies to small vacancy clusters was observed in tungsten at 400 °C using field ion microscopy [38]. Therefore, we can expect that a significant amount of the initial interstitial loops have disappeared during heating the W-5Ta sample up to 500 °C, and the structure is characterized by the presence of additional vacancy-type $a/2\langle 111 \rangle$ dislocation loops. At that temperature, the loop density amounts to $1.5 \times 10^{21} \text{ m}^{-3}$ and the average loop size to $28(2)$ nm. A step-wise increase in annealing temperature above 500 °C causes a progressive reduction in loop density, which levels off at temperatures close to

900 °C, see Fig. 2. Vacancy-type defects become mobile in this temperature regime, which corresponds to annealing stage IV reported to occur at 650 – 1000 °C [28]. This trend in loop characteristics evidences the growth of vacancy-type loops by loop and vacancy absorption and, to a lesser degree, by loop coalescence [39]. At 900 °C the loop

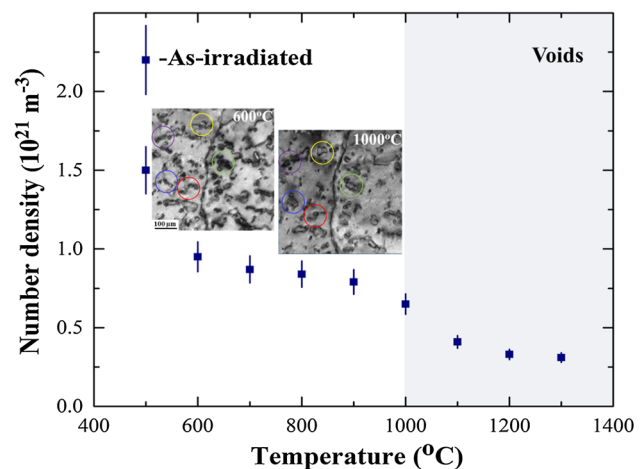


Fig. 2 Variation in the number density of dislocation loops in W-5Ta alloy during post irradiation annealing up to 1300 °C. The coloured region of the graph represents the temperature range where voids are present in the microstructure during annealing. Inset TEM images show evidence of dislocation loop absorption with increasing temperature

density equals to $0.8 \times 10^{21} \text{ m}^{-3}$ and the average loop size to 26(2) nm.

Void Formation

Annealing the sample at temperatures above 900 °C reveals a second progressive decrease in loop density, see Fig. 2. This overlaps with the annealing stage V, whose onset is reported to occur at 1000 °C in tungsten [28]. This stage is characterised by the thermal dissociation of vacancies from lattice defects such as dislocation loops. Furthermore, we have also observed the occurrence of a significant number of voids in the microstructure at a temperature of 1000 °C, see Fig. 3. At that temperature, the void number density amounts to $5.8 \times 10^{21} \text{ m}^{-3}$. An increase in temperature beyond 1000 °C causes a decrease in the number density of voids, and concomitantly to an increase in the average void diameter, see Fig. 4. The average number of vacancies per void (n), assuming a spherical shape of the voids, can be estimated using the expression [40]:

$$n = \frac{4\pi R_v^3}{3\Omega} \quad (1)$$

where R_v denotes the average void radius and Ω the atomic volume. The values obtained for n as a function of the annealing temperature are shown in the inset of Fig. 4b. At the highest annealing temperature of 1300 °C in this study, the average number of vacancies per void is $n \sim 18 \times 10^3$, and the void number density is $1.2 \times 10^{21} \text{ m}^{-3}$. Voids are formed either by the clustering of free vacancies, or by the shrinkage and collapse of vacancy-type dislocation loops via vacancy emission [41]. Once voids reach a critical size, they are stable and increase their size by absorbing additional mobile vacancies from the matrix. In fact, mesoscopic vacancy-type dislocation loops are predicted to be metastable with respect to the transformation into spherical voids [42]. Radiation-induced void swelling takes place in neutron irradiated tungsten in the temperature range of 600–900 °C at a damage level of $\sim 9.5 \text{ dpa}$ [43]. Voids are reported to form in tungsten at an early stage of irradiation, and a void lattice appears at a

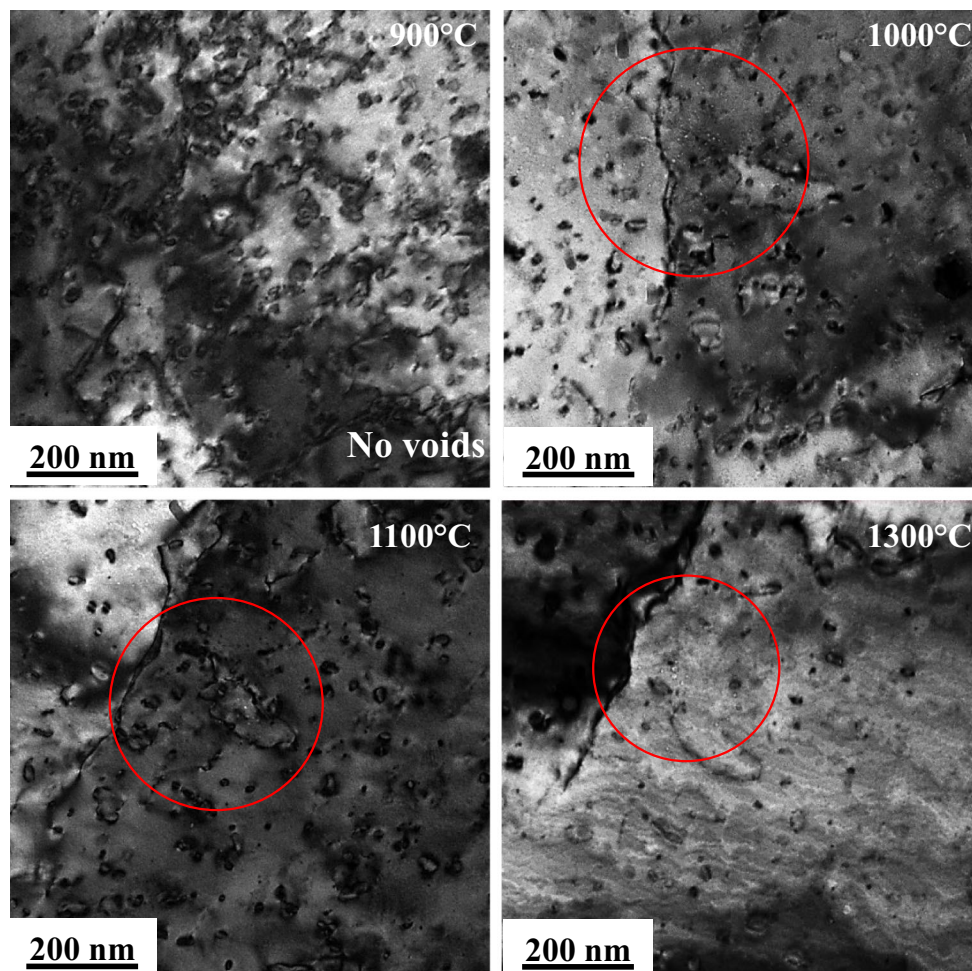


Fig. 3 Occurrence and evolution of voids in proton irradiated W-5Ta alloy during annealing

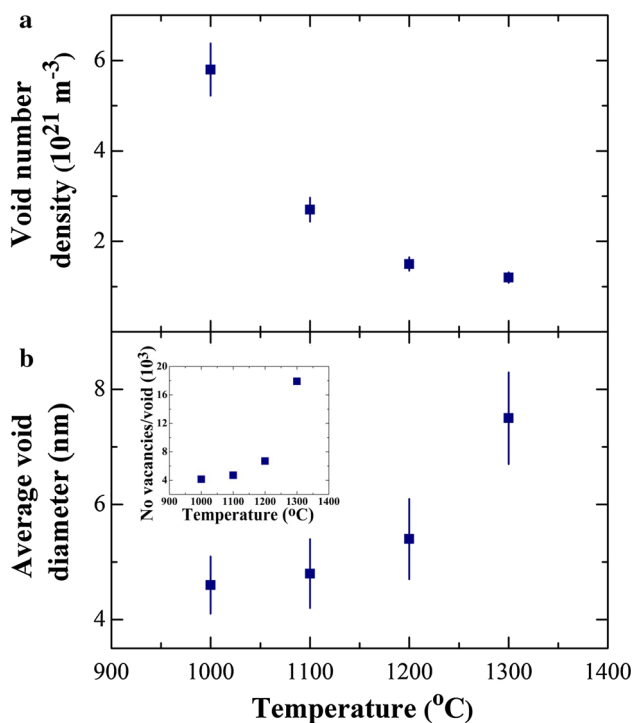


Fig. 4 Number density and average diameter of voids formed in irradiated W-5Ta alloy as a function of annealing temperature. The inset in **b** shows the dependence of the average number of vacancies per void on the annealing temperature (see text)

damage level of ~ 1 dpa at temperatures of 600–800 °C. Moreover, once a void lattice is formed in tungsten, it is expected to remain stable at higher dpa level [44]. We have observed the appearance of voids visible by TEM in W-5Ta alloy at a higher temperature, i.e. 1000 °C, as compared to tungsten. Tantalum constitutes an oversized atom in tungsten, and can reduce the free vacancy concentration in the matrix via a solute-trapping mechanism [45], therefore delaying or reducing the void formation and the related swelling in W-5Ta alloy as compared to tungsten.

Conclusions

To summarize, the microstructure of W-5Ta alloy after 40 keV proton irradiation at 350 °C and a damage level of 0.7 dpa is characterized by the presence of interstitial-type $a/2\langle 111 \rangle$ dislocation loops. The in-situ post-irradiation annealing of W-5Ta in a TEM causes those interstitial loops to emit SIAs and also to glide to the free surface of the sample. The resultant excess of vacancies in the matrix evolves into vacancy-type $a/2\langle 111 \rangle$ dislocation loops, which grow preferentially by loop and vacancy absorption in the temperature range of 600–900 °C. At a temperature of 1000 °C a significant number of voids appear in the

microstructure, whereas the loop number density decreases. The void number density reduces gradually up to a temperature of 1300 °C, and the average void diameter increases simultaneously. Tantalum delays the onset of void formation in W-5Ta alloy, as compared to tungsten, via a solute-vacancy trapping mechanism.

Acknowledgements The work described was supported by the Dalton Cumbrian Facility Project, a joint facility of The University of Manchester and the Nuclear Decommissioning Authority. The authors are also acknowledge access to the MIAMI facility through the EPSRC funded UK national ion beam centre.

Open Access This article is distributed under the terms of the Creative Commons Attribution 4.0 International License (<http://creativecommons.org/licenses/by/4.0/>), which permits unrestricted use, distribution, and reproduction in any medium, provided you give appropriate credit to the original author(s) and the source, provide a link to the Creative Commons license, and indicate if changes were made.

References

1. M. Rieth, S.L. Dudarev, S.M. Gonzalez de Vicente, J. Aktaa, T. Ahlgren, S. Antusch et al., *J. Nucl. Mater.* **442**, S173 (2013)
2. S. Wurster, N. Baluc, M. Battabyal, T. Crosby, J. Du, C. García-Rosales et al., *J. Nucl. Mater.* **442**, S181 (2013)
3. R. Neu, J. Riesch, J.W. Coenen, J. Brinkmann, A. Calvo, S. Elgeti et al., *Fusion Eng. Des.* **109–111**, 1046 (2016)
4. D.M. Duffy, *Philos. Trans. R. Soc. A* **368**, 3315 (2010)
5. T. Shen, Y. Dai, Y. Lee, *J. Nucl. Mater.* **468**, 348 (2016)
6. M. Wirtz, I. Uytendhouwen, V. Barabash, F. Escourbiac, T. Hirai, J. Linke et al., *Nucl. Fusion* **57**, 066018 (2017)
7. L. Giancarli, J.P. Bonal, A. Li Puma, B. Michel, P. Sardain, J.F. Salavy, *Fusion Eng. Des.* **75–79**, 383 (2005)
8. N. Baluc, *Phys. Scr.* **T138**, 014004 (2009)
9. B. Bazyleva, G. Janeschitz, I. Landman, S. Pestchanyi, A. Loarte, G. Federici et al., *Fusion Eng. Des.* **83**, 1077 (2008)
10. T. Shen, Y. Dai, Y. Lee, *J. Nucl. Mater.* **468**, 348 (2016)
11. V. Philipps, *J. Nucl. Mater.* **415**, 52 (2011)
12. H. Bolt, V. Barabash, G. Federici, J. Linke, A. Loarte, J. Roth, K. Sato, *J. Nucl. Mater.* **307–311**, 43 (2002)
13. S.J. Zinkle, N.M. Ghoniem, *Fusion Eng. Des.* **51–52**, 55 (2000)
14. G.A. Cottrell, *J. Nucl. Mater.* **334**, 166 (2004)
15. A. Hasegawa, M. Fukuda, T. Tanno, S. Nogami, *Mater. Trans.* **54**, 466 (2013)
16. Ph Mertens, V. Thompson, G.F. Matthews, D. Nicolai, G. Pintuk, V. Riccardo et al., *J. Nucl. Mater.* **438**, S401 (2013)
17. D. Jiang, Q. Wang, W. Hu, Z. Wei, J. Tong, H. Wan, *J. Mater. Res.* **31**, 3401 (2016)
18. A. Xu, D.E.J. Armstrong, C. Beck, M.P. Moody, G.D.W. Smith, P.A.J. Bagot et al., *Acta Mater.* **124**, 71 (2017)
19. X. Yi, M.L. Jenkins, K. Hattar, P.D. Edmondson, S.G. Roberts, *Acta Mater.* **92**, 163 (2015)
20. D.E.J. Armstrong, A.J. Wilkinson, S.G. Roberts, *Phys. Scr.* **T145**, 014076 (2011)
21. M. Muzyk, D. Nguyen-Manh, K.J. Kurzydłowski, N.L. Baluc, S.L. Dudarev, *Phys. Rev. B* **84**, 104115 (2011)
22. W. Setyawan, G. Nandipati, R.J. Kurtz, *J. Nucl. Mater.* **484**, 30 (2017)
23. J.A. Hinks, J.A. van den Berg, S.E. Donnelly, *J. Vac. Sci. Technol. A* **29**, 21003 (2011)

24. M.L. Jenkins, M.A. Kirk, *Characterization of Radiation Damage by Transmission Electron Microscopy* (IOP Publishing Ltd, Bristol, 2001)
25. B.N. Singh, J.H. Evans, J. Nucl. Mater. **226**, 277 (1995)
26. R.M. Scanlan, D.L. Styrus, D.N. Seidman, Philos. Mag. **23**, 1459 (1971)
27. F. Dausinger, H. Schultz, Phys. Rev. Lett. **35**, 1773 (1975)
28. L.K. Keys, J. Moteff, J. Nucl. Mater. **34**, 260 (1970)
29. R.M. Scanlan, D.L. Styrus, D.N. Seidman, Philos. Mag. **23**, 1439 (1971)
30. D.I.R. Norris, Radiat. Eff. **15**, 1 (1972)
31. F. Ferroni, E. Tarleton, S. Fitzgerald, Model. Simul. Mater. Sci. Eng. **22**, 045009 (2014)
32. F. Ferroni, X. Yi, K. Arakawa, S.P. Fitzgerald, P.D. Edmondson, S.G. Roberts, Acta Mater. **90**, 380–393 (2015)
33. M. Kiritani, Mater. Sci. Forum **15–18**, 1023 (1987)
34. D.N. Seidman, Scr. Metall. **13**, 251 (1979)
35. L.K. Keys, J.P. Smith, J. Moteff, Scr. Metall. **1**, 71 (1967)
36. M.W. Thompson, Philos. Mag. **5**, 278 (1960)
37. H. Schultz, Scr. Metall. **8**, 721 (1974)
38. K.M. Bowkett, B. Ralph, Proc. R. Soc. A **312**, 51 (1969)
39. X. Yi, M.L. Jenkins, M. Briceno, S.G. Roberts, Z. Zhou, M. Kirk, Philos. Mag. **93**, 1715 (2013)
40. G. Was, *Fundamentals of Radiation Materials Science* (Springer, New York, 2007)
41. B.L. Eyre, D.M. Maher, Philos. Mag. **24**, 767 (1971)
42. M.R. Gilbert, S.L. Dudarev, P.M. Derlet, D.G. Pettifor, J. Phys. Condens. Matter **20**, 345214 (2008)
43. J. Matolich, H. Nahm, J. Moteff, Scr. Metall. **8**, 837 (1974)
44. A. Hasegawa, M. Fukuda, S. Nogami, K. Yabuuchi, Fusion Eng. Des. **89**, 1568 (2014)
45. F.A. Smidt, J.A. Sprague, Scr. Metall. **7**, 495 (1973)